

Article

Not peer-reviewed version

Non-invasive Monitoring of Cerebral Edema Using Ultrasonic Echo Signal Features and Machine Learning

[Shuang Yang](#), Yuanbo Yang, [Yufeng Zhou](#) *

Posted Date: 30 October 2024

doi: 10.20944/preprints202410.2440.v1

Keywords: cerebral edema; ultrasonic echo signal; non-invasive monitoring; machine learning



Preprints.org is a free multidisciplinary platform providing preprint service that is dedicated to making early versions of research outputs permanently available and citable. Preprints posted at Preprints.org appear in Web of Science, Crossref, Google Scholar, Scilit, Europe PMC.

Copyright: This open access article is published under a Creative Commons CC BY 4.0 license, which permit the free download, distribution, and reuse, provided that the author and preprint are cited in any reuse.

Article

Non-invasive Monitoring of Cerebral Edema Using Ultrasonic Echo Signal Features and Machine Learning

Shuang Yang ^{1,2}, Yuanbo Yang ^{1,2} and Yufeng Zhou ^{1,2,3*}

¹ State Key Laboratory of Ultrasound in Medicine and Engineering, Chongqing Medical University, Chongqing, 400016, China

² Chongqing Key Laboratory of Biomedical Engineering, Chongqing Medical University, Chongqing, 400016, China

³ National Medical Products Administration (NMPA) Key Laboratory for Quality Evaluation, Ultrasonic Surgical Equipment, 507 Gaoxin Ave., Donghu New Technology Development Zone, Wuhan, 430075, Hubei, China

* Correspondence: yufeng.zhou@cqum.edu.cn

Abstract: Objectives: Cerebral edema, a prevalent consequence of brain injury, is associated with significant mortality and disability. Timely diagnosis and monitoring are crucial for patient prognosis. There is a pressing clinical demand for a real-time, non-invasive cerebral edema monitoring method. Ultrasound methods are prime candidates for such investigations due to their non-invasiveness nature; **Methods:** Acute cerebral edema by permanently occluding the left middle cerebral artery (MCA) was introduced in rats. Ultrasonic echo signals were collected at nine time points over a 24-hour period to extract features from both the time and frequency domains. Concurrently, histomorphological changes were examined. We utilized support vector machine (SVM), logistic regression (LR), decision tree (DT), and random forest (RF) algorithms for classifying cerebral edema types, and SVM, RF, and feedforward neural network (FNN) for predicting the cerebral infarction volume ratio; **Results:** The integration of 16 ultrasonic features associated with cerebral edema development with the RF model enabled effective classification of cerebral edema types with a high accuracy rate of 97.9%. Additionally, it provided an accurate prediction of the cerebral infarction volume ratio, with an R^2 value of 0.8814; **Conclusions:** Our proposed strategy classifies cerebral edema and predicts the cerebral infarction volume ratio with satisfactory precision. The fusion of ultrasound echo features with machine learning presents a promising non-invasive approach for the monitoring of cerebral edema.

Keywords: cerebral edema; ultrasonic echo signal; non-invasive monitoring; machine learning

1. Introduction

Cerebral edema is a pathological state characterized by an increase in brain volume due to abnormal increase or accumulation of intracranial fluid [1]. Cerebral edema is often a complication of traumatic brain injury, stroke, and other craniocerebral diseases, and cerebral edema can lead to elevated intracranial pressure (ICP), causing neurological deficits, brain displacement, or herniation [2]. In extreme cases, it poses a serious threat to life. The etiology of cerebral edema is intricate, with two primary types: cytotoxic and vasogenic cerebral edema [3]. Cytotoxic cerebral edema typically predominates initially, while vasogenic cerebral edema takes over later [4]. This distinction is crucial, as it influences treatment strategies [5,6]. Therefore, timely classification and ongoing monitoring of cerebral edema are essential for improving diagnostic precision and therapeutic efficiency.

Currently available methods have certain limitations. Invasive ICP monitoring, which involves the insertion of pressure sensors into the brain parenchyma, ventricles, or subdural space, only indirectly indicating the severity of cerebral edema [7]. However, the probe is prone to shift during

monitoring, diminishing the monitoring accuracy, and carries risk of intracranial hemorrhage or infection [8–10]. Lietke et al. correlated computed tomography (CT)-based cerebral edema classification with ICP ($r = 0.51$, $p < 0.0001$) [9]. Electrical impedance tomography (EIT), another invasive method, measures electrical impedance differences to assess cerebral edema progression [10], but it lacks the ability to quantify edema severity. Non-invasive imaging techniques like CT and magnetic resonance imaging (MRI) accurately delineate edema characteristics and depict its location [11]. However, their limitations, including size, cost, and ionizing radiation risks, make them unsuitable for real-time, continuous monitoring at bedside. Near-infrared spectroscopy (NIRS) has been explored for early detection of cerebral edema before ICP increases [12], and magnetic induction phase shift (MIPS) technology has shown promise in distinguishing between cytotoxic and vasogenic cerebral edema with high sensitivity and anti-interference capabilities [13]. While these studies highlight the potential for cerebral edema monitoring, advancements and practical applications are still required.

Ultrasound, with the advantages of non-invasiveness, repeatability, and absence of ionizing radiation, is valuable for monitoring or diagnosing ICP, cerebral blood flow, hydrocephalus, intracranial hematomas, and midline shift (MLS) of the brain, among other cranial conditions [14–16]. Transcranial color-coded Doppler (TCCD) has been shown to accurately detect intracranial hemorrhage or ischemic stroke with a sensitivity of 94%, and specificity of 95%, closely matching with CT results [15]. Furthermore, ultrasound has also demonstrated good agreement with CT in assessing MLS in neurocritical care patients ($r = 0.65$, $p < 0.001$) [16].

During cerebral edema, brain tissue properties like density and hardness change, affecting the acoustic impedance of the intracranial brain tissue and ultrasound propagation inside it. It is hypothesized that ultrasound echo features are correlated with the types and severity of cerebral edema. In this study, a non-invasive method of monitoring cerebral edema was introduced using ultrasonic echo signal features. Firstly, a cerebral edema model was established by permanently occluding the left MCA in rats. Then, the ultrasonic echo signals were recorded over 24 hours to extract the features of waveform and spectrum. And the morphology of cerebral edema was quantitatively analyzed. Finally, selected features were input into machine learning models to classify cerebral edema types and predict cerebral infarction volume ratios.

2. Materials and Methods

2.1. Experimental Animals and Grouping

Sixty healthy adult Sprague-Dawley (SD) rats weighing 250 ± 20 g without specific pathogens or infections, and evenly divided by sex, were obtained from the Animal Experiment Center of Chongqing Medical University. The research protocol was approved and supervised by the Institutional Animal Care and Use Committee (IACUC) of Chongqing Medical University (IACUC-CQMU-2024-0698). The study adhered to the Guide in the Care and Use of Laboratory Animals established by the U.S. National Academy of Sciences. The rats were maintained in a temperature-controlled environment of 20–25 °C, under a 12/12-hour light-dark cycle, with ad libitum access to food and water. They were randomly assigned to three groups: (1) 20 rats with cerebral edema and 3 with sham surgery controls were monitored using ultrasound echoes before and at nine postoperative time points within 24 hours (0, 1, 2, 3, 6, 9, 12, 18, and 24 hours); (2) 27 rats were used for 2,3,5-triphenyltetrazolium chloride (TTC) staining at each time point (3 rats per point); (3) 10 rats were utilized for histological assessment.

2.2. Cerebral Ischemia Model

Rats were deprived of food and water for 12 hours prior to surgery. Following anesthesia induction with pentobarbital sodium (1.5%, 0.2 ml/100 g, P3761, Sigma-Aldrich, St. Louis, MO), a permanent cerebral ischemia model was established via middle cerebral artery occlusion (MCAO) using a silicone thread plug (45-0480, Hengqinda, Shanghai, China) [17,18]. A 1.5–2 cm neck incision was made 1 cm away the left of the midline, and the left common carotid artery (CCA), external

carotid artery (ECA), and internal carotid artery (ICA) were carefully isolated along the sternocleidomastoid muscle. The vagus nerve was meticulously separated to prevent injury that could affect respiration and swallowing. The proximal end of CCA and the origin of ECA were ligated with surgical thread, and a hemostatic clamp and surgical threads were positioned at the origin of ICA and distal end of CCA, respectively. An incision was made about 5 mm between the CCA's end and the carotid bifurcation. A silicone thread plug was inserted in the direction of CCA, advancing 1-2 mm into ICA after releasing the hemostatic clamp. The blood supply to the brain was obstructed by tightening the thread with the prepared surgical thread. Finally, the incision was closed, and rats were placed on a 37 °C thermostatic heating pad for recovery.

2.3. Assessment of Neurological Deficits

Neurological deficits were assessed two hours post-ischemia using the Zea-Longa method [19]: 0 = no deficits; 1 = inability to extend the uninjured forelimb; 2 = walking towards the undamaged side; 3 = turning toward the undamaged side in a rear-end shape; 4 = consciousness disturbance, no independent ambulation. Scores between 1 and 3 indicate successful modeling; otherwise, the rats were discarded.

2.4. Analysis of Cerebral Infarction Volume

After the rats were anesthetized, their hearts were perfused with normal saline. Then, brains were quickly extracted and refrigerated at -20 °C for 25 minutes. The cerebellum and other parts were removed to retain the brain tissue only, and five coronal sections in a thickness of about 2 mm were prepared. These sections were incubated in a 2% solution of TTC (Solarbio, Beijing, China) at 37 °C for 30 minutes and then fixed in 4% paraformaldehyde (PFA) solution (Biosharp, Anhui, China) for 5 hours in the dark. The infarct volume was analyzed using Image J software (National Institute of Health, Bethesda, MD), with the ratio calculated as [20]:

$$\text{infarction volume ratio} = \left(\frac{\text{volume of the contralateral hemisphere} - \text{unstained volume of the ipsilateral hemisphere}}{\text{volume of the contralateral hemisphere}} \right) \times 100\% \quad (1)$$

2.5. Assessment of Histology

Following anesthesia, rats were perfused with normal saline, and brains were rapidly removed and fixed in 4% PFA for 24 hours. Paraffin sections of 3-4 µm thick were stained with hematoxylin (H9627, Sigma-Aldrich)-eosin (E4009, Sigma-Aldrich) (HE) and examined under a 200× upright microscope (Eclipse Ci-L, Nikon, Tokyo, Japan).

2.6. Ultrasonic Echo Signal Acquisition

Figure. 1a shows the ultrasonic echo signal acquisition system in this study. The rats' heads were shaved, and ultrasonic coupling gel was evenly applied. A 2.25 MHz flat ultrasound transducer (V306-SU, Olympus, Waltham, MA) was used with a pulse transmitter receiver (DPR300, BYK-Gardner, NY) to emit and receive ultrasonic waves, which were acquired by an oscilloscope (DHO4000, RIGOL, Suzhou, Jiangsu, China) at the sampling rate of 500 MSa/s, averaged 64 times. The ultrasound transducer was positioned over the left parietal bone, and four data were collected at each time point.

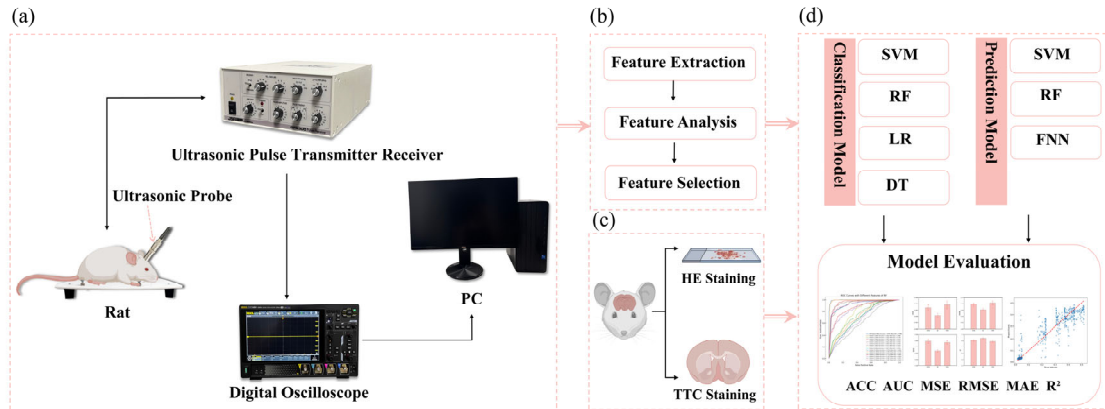


Figure 1. Flowchart of research framework: (a) acquisition of ultrasonic echos from cerebral edema rats, (b) extraction, analysis, and selection of ultrasonic features, (c) HE and TTC staining of cerebral edema rats, and (d) classification of cerebral edema types and prediction of cerebral infarction volume ratio.

2.7. Feature Parameter Extraction

The acquired ultrasound echos were processed to remove the DC component and then transformed into frequency domain using Fourier analysis. Subsequently, MATLAB (R2022a, MathWorks, Natick, MA) was used to extract 13 time-domain features (maximum, minimum, mean, peak-to-peak, absolute average, variance, standard deviation, kurtosis, skewness, root mean square, shape factor, impulse factor, and crest factor) and 9 frequency-domain features (mean magnitude in the frequency domain, centroid frequency, mean square frequency, variance frequency, frequency variance, mean frequency, total power, average power, and peak frequency) as listed in Table 1. These features were compiled into a dataset.

Table 1. Features of ultrasonic echo signal in the time and frequency domain.

| Feature | Formula | Feature | Formula |
|--------------------|--|--|---|
| Maximum | $F_1 = \max(x)$ | Impulse Factor | $F_{12} = \frac{F_4}{F_5}$ |
| Minimum | $F_2 = \min(x)$ | Crest Factor | $F_{13} = \frac{F_4}{F_{10}}$ |
| Mean | $F_3 = \frac{1}{N} \sum_{i=1}^n x_i$ | Mean Magnitude In The Frequency Domain | $F_{14} = \frac{1}{N} \sum_{i=1}^n A(f_i)$ |
| Peak-to-Peak | $F_4 = F_1 - F_2$ | Centroid Frequency | $F_{15} = \frac{\sum_{i=1}^n f_i \cdot A(f_i)}{\sum_{i=1}^n A(f_i)}$ |
| Average | $F_5 = \frac{1}{N} \sum_{i=1}^n x_i $ | Mean squared frequency | $F_{16} = \frac{\sum_{i=1}^n f_i^2 \cdot A(f_i)}{\sum_{i=1}^n A(f_i)}$ |
| Variance | $F_6 = \frac{1}{N-1} \sum_{i=1}^n (x_i - F_3)^2$ | Variance frequency | $F_{17} = \sqrt{F_{16}}$ |
| Standard Deviation | $F_7 = \sqrt{F_6}$ | Frequency variance | $F_{18} = \frac{\sum_{i=1}^n (f_i - F_{15})^2 \cdot A(f_i)}{\sum_{i=1}^n A(f_i)}$ |
| Kurtosis | $F_8 = \frac{\frac{1}{N} \sum_{i=1}^n (x_i - F_3)^4}{F_7^4}$ | Mean Frequency | $F_{19} = \frac{\sum_{i=1}^n f_i \cdot P(f_i)}{\sum_{i=1}^n P(f_i)}$ |
| Skewness | $F_9 = \frac{\frac{1}{N} \sum_{i=1}^n (x_i - F_3)^3}{F_7^3}$ | Total Power | $F_{20} = \sum_{i=1}^n P(f_i)$ |

| | | | |
|------------------|--|----------------|--|
| Root Mean Square | $F_{10} = \sqrt{\frac{1}{N} \sum_{i=1}^n x_i^2}$ | Average Power | $F_{21} = \frac{1}{N} \sum_{i=1}^n P(f_i)$ |
| Shape Factor | $F_{11} = \frac{F_{10}}{F_5}$ | Peak frequency | $F_{22} = f_{\arg \max_j P(f_j)}$ |

2.8. Classification of Cerebral Edema and Model Evaluation

Python 3.12 and PyCharm 2023.1 were employed for data analysis. The ultrasound features dataset were refined using the z-score method, which involved replacing outliers with the median, filling in missing values with the mean, and normalizing the data [21]. Four traditional machine learning models including support vector machine (SVM), logistic regression (LR), decision tree (DT) and random forest (RF) were used to classify cerebral edema. Such classification is based on a single feature and sixteen features, respectively. To fully evaluate the classification performance, a 10-fold cross validation was conducted to assess the average accuracy (ACC) and the average area curve (AUC) under the receiver operating characteristic (ROC).

2.9. Prediction of Cerebral Infarction Volume Ratio and Model Evaluation

Spline interpolation was used to address the data imbalance between ultrasound features and cerebral infarction volume ratios. SVM, RF, and feedforward neural network (FNN) were trained to predict the volume ratio of cerebral infarction. To prevent overfitting, 10-fold cross validation was performed to determine the average values of root mean square error (RMSE), mean square error (MSE), mean absolute error (MAE) and R^2 as the evaluation indexes. The SVM model applied a linear kernel with the regularization parameter (C) of 1. RF hyperparameters included 100 trees, a maximum depth of 20, and the minimum 5 samples and 1 sample required to split an internal and leaf node, respectively. The FNN model employed ReLU activation function with two fully connected layers (64 and 32 neurons), Adam optimizer, MSE loss function, a learning rate of 0.001, 50 training epochs, and a batch size of 64.

2.10. Statistical Analysis

Statistical analysis was conducted using Origin software (2024, OriginLab, Northampton, MA). Non-parametric Kruskal-Wallis analysis and Dunn's post-hoc test were applied to compare the features at each time point, with $p < 0.05$ indicating statistical significance.

3. Results

3.1. Changes to Features Over Time

Figure 2 shows the boxplots of 16 features, highlighting significant differences between the initial (0 hour) and final (24 hours) time points ($p < 0.001$), including maximum, minimum, peak-to-peak, absolute average, variance, standard deviation, kurtosis, skewness, root mean square, shape factor, impulse factor, crest factor, mean magnitude in the frequency domain, mean frequency, total power, and average power. The majority of these features remained stable within the first three hours post-hemorrhagic brain injury. However, a noticeable decline was observed between 3 and 24 hours post-ischemic brain injury, with the exception of a rising trend in the minimum value. Except for kurtosis at the 6 hour ($p = 0.393$), all features from 6 to 24 hours varied significantly from the initial state ($p < 0.001$). Notably, features from the pre-modeling phase and control group did not diverge until the 6, 9, 12, 18, and 24-hour marks ($p < 0.001$).

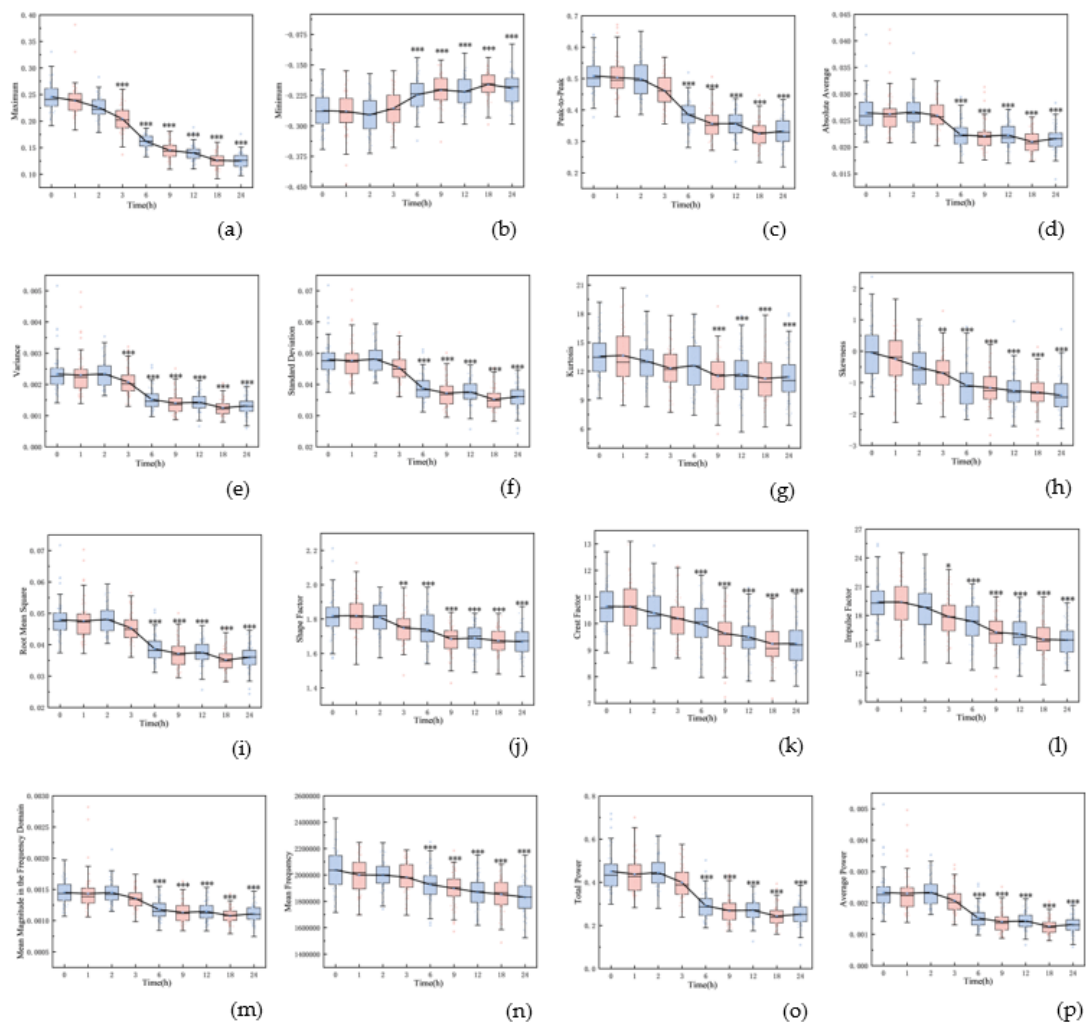


Figure 2. Boxplots of 16 features over time (*: $p < 0.05$, **: $p < 0.01$, ***: $p < 0.001$).

3.2. Volume Ratio of Cerebral Infarction over Time

Neurological deficits were markedly evident in rats 2 hours post-permanent cerebral ischemia, with a neurological score of 2.66 ± 0.48 . Figure 3 illustrates representative TTC staining results at nine time points, differentiating normal (red) from ischemic (white) brain tissue. The infarcted area of ischemic brain tissue increased substantially over time. As depicted in Figure 4, the infarction volume ratio was minimally altered in the first 3 hours, subsequently reaching 48.2% by the 24-hour mark.

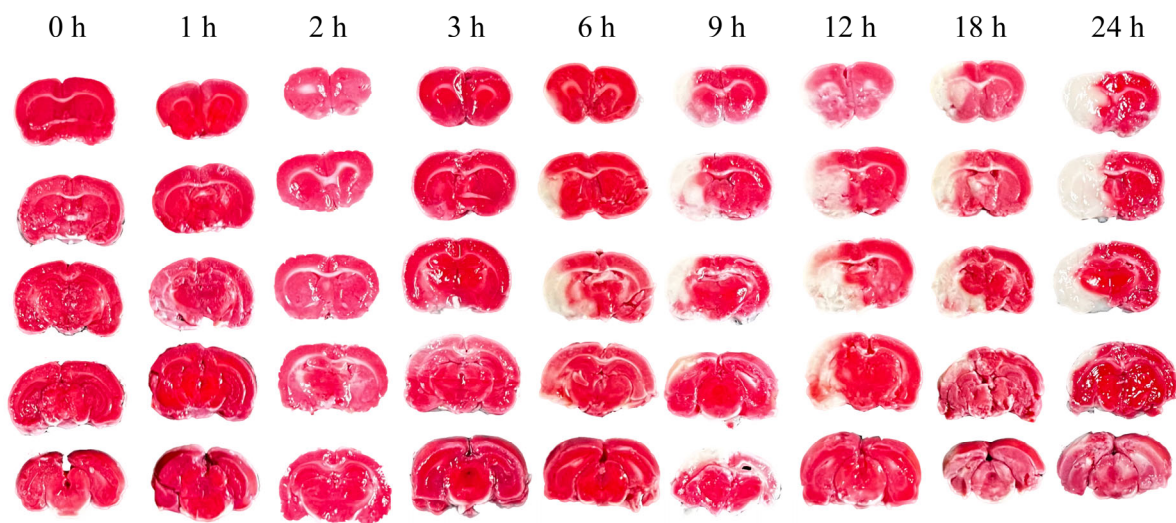


Figure 3. Representative TTC staining of rat brain at nine time points.

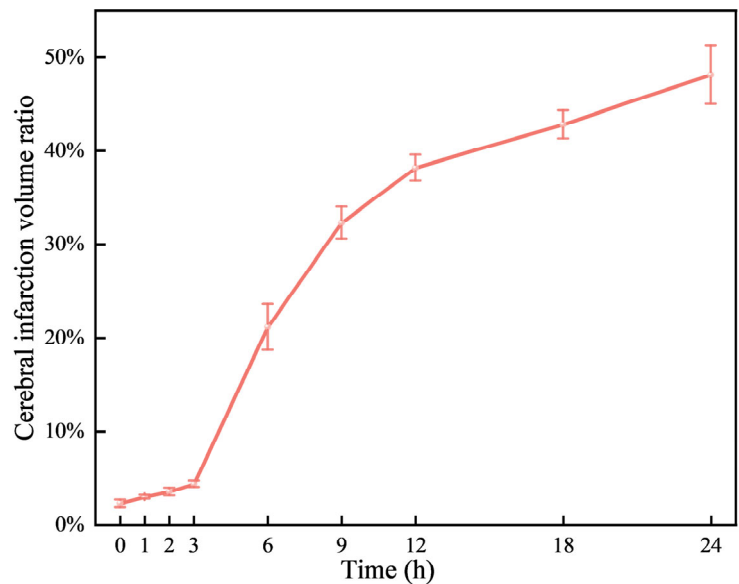


Figure 4. Variations of cerebral infarction volume ratio over time.

3.3. *Pathological Morphology at Different Time*

Examination under a 200× upright microscope revealed the microstructure of brain tissue, as shown in Figure 5. At 0 hours, no significant abnormalities were observed, all neurons appearing intact and neatly arranged without signs of swelling or necrosis (see Figure 5a). In contrast, 3 hours post-MCAO, ischemic brain tissue showed disordered neuronal arrangement and significantly enlarged neuron volume (see Figure 5b). Nuclei appeared hyperchromatic with evident nuclear pyknosis and degeneration, indicating early cerebral edema. By 9 hours, nuclear pyknosis became more pronounced, with shrunken neuronal cell bodies, enlarged intercellular spaces, and expanded perivascular spaces by fluid exudation, suggesting worsening edema and vasogenic changes (see Figure 5c). At 24 hours, extensive neuronal necrosis was apparent, with edematous vacuoles, reduced cell density, and enlarged tissue gaps, indicative of severe cerebral edema (see Figure 5d).

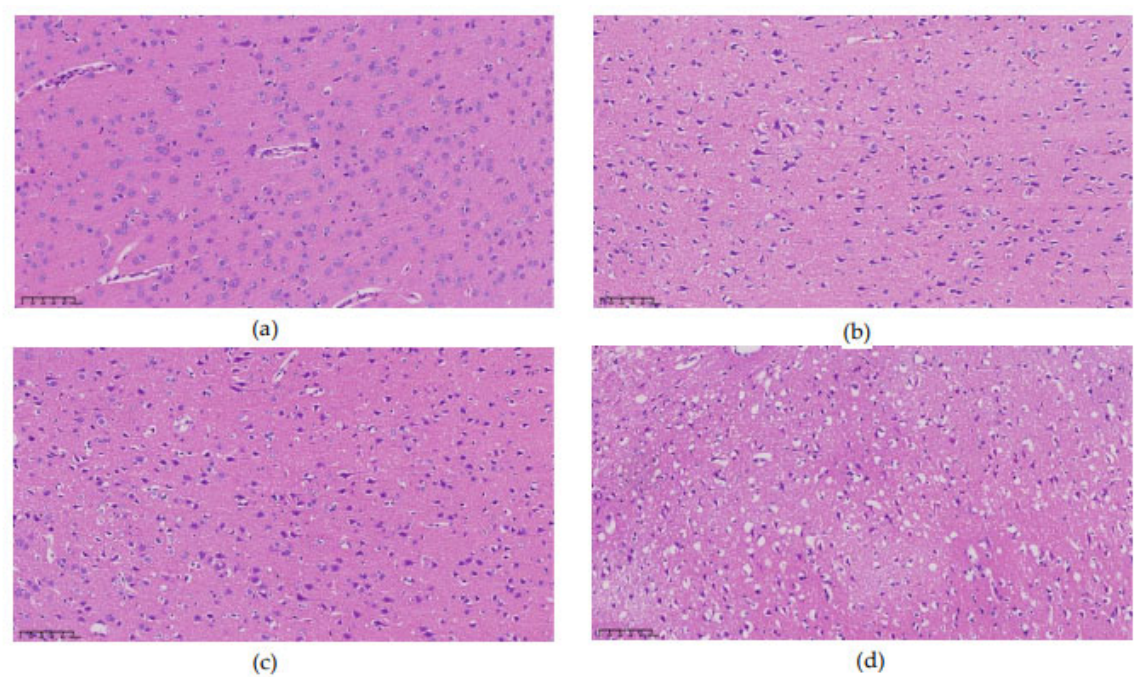


Figure 5. Microscopic structure of representative (a, b, c, d) cerebral edema tissue at 0 hour, 3 hour, 9 hour, and 24 hour under an upright microscope at 200×, respectively.

3.4. Cerebral Edema Classification

In this study, SVM, RF, LR, and DT were selected to compare their performance in classifying cerebral edema using 16 features as listed in Table 2. All models demonstrated high classification accuracy, with ACC of $96.7\pm3.4\%$, $97.9\pm1.9\%$, $97.2\pm3.0\%$, and $95.8\pm2.1\%$, respectively. Their AUCs were 0.996 ± 0.007 , 0.996 ± 0.005 , 0.997 ± 0.005 , and 0.959 ± 0.022 , respectively. It is worth noting that when classifying with a single feature, the yielded prediction across all four models is quite satisfactory, with the ACC of $97.5\%\pm1.7\%$, $96.3\%\pm2.2\%$, $97.2\%\pm3.0\%$, and $96.3\%\pm2.2\%$, respectively and the AUC of 0.993 ± 0.010 , 0.988 ± 0.011 , 0.996 ± 0.006 , and 0.962 ± 0.023 , respectively (see Figure 6).

Table 1. Classification of cerebral edema using the four models.

| Model | ACC | AUC |
|-------|-----------------|-----------------|
| SVM | 0.967 ± 0.034 | 0.996 ± 0.007 |
| RF | 0.979 ± 0.019 | 0.996 ± 0.005 |
| LR | 0.972 ± 0.030 | 0.997 ± 0.005 |
| DT | 0.958 ± 0.021 | 0.959 ± 0.022 |

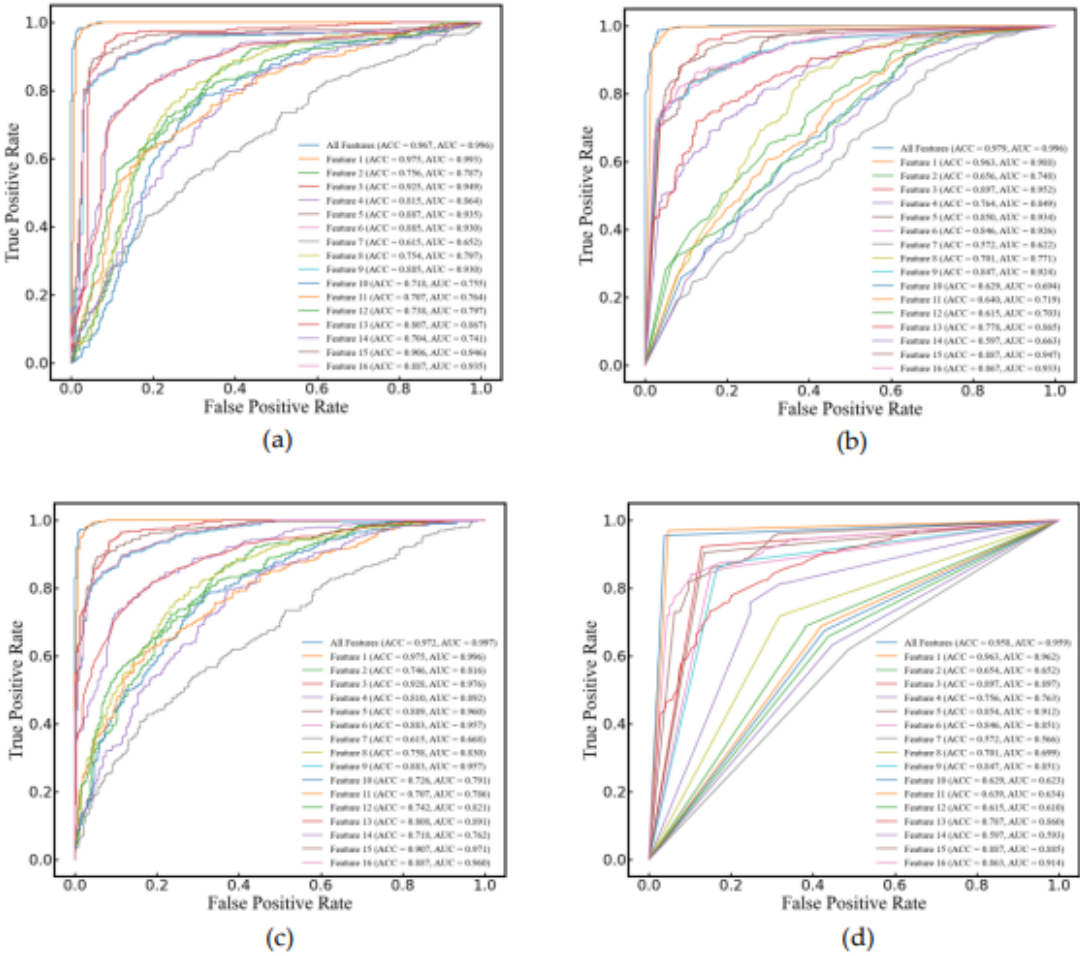


Figure 6. ROC curves of single feature and 16 features for classifying cerebral edema.

3.5. Prediction of Cerebral Infarction Volume Ratio

Comparing the predictive performance (MSE, RMSE, and MAE) of three methods on the infarction volume ratio, RF outperformed in terms of generalization and stability, the MSE, RMSE, and MAE of 0.0038 ± 0.0006 , 0.0612 ± 0.0046 , and 0.0379 ± 0.0035 , respectively, as shown in Table 3 and Figure 7. Additionally, the correlation between RF-predicted and actual infarction volume ratio was quite substantial ($R^2 = 0.8814\pm0.0223$), as shown in Figure 8.

Table 3. Predictive performance of three models for cerebral infarction volume ratio.

| Model | MSE | RMSE | MAE | R ² |
|-------|---------------|---------------|---------------|----------------|
| SVM | 0.0061±0.0008 | 0.0782±0.0048 | 0.0632±0.0054 | 0.8079±0.0268 |
| RF | 0.0038±0.0006 | 0.0612±0.0046 | 0.0379±0.0035 | 0.8814±0.0223 |
| FNN | 0.0066±0.0015 | 0.0808±0.0091 | 0.0577±0.0066 | 0.7929±0.0506 |

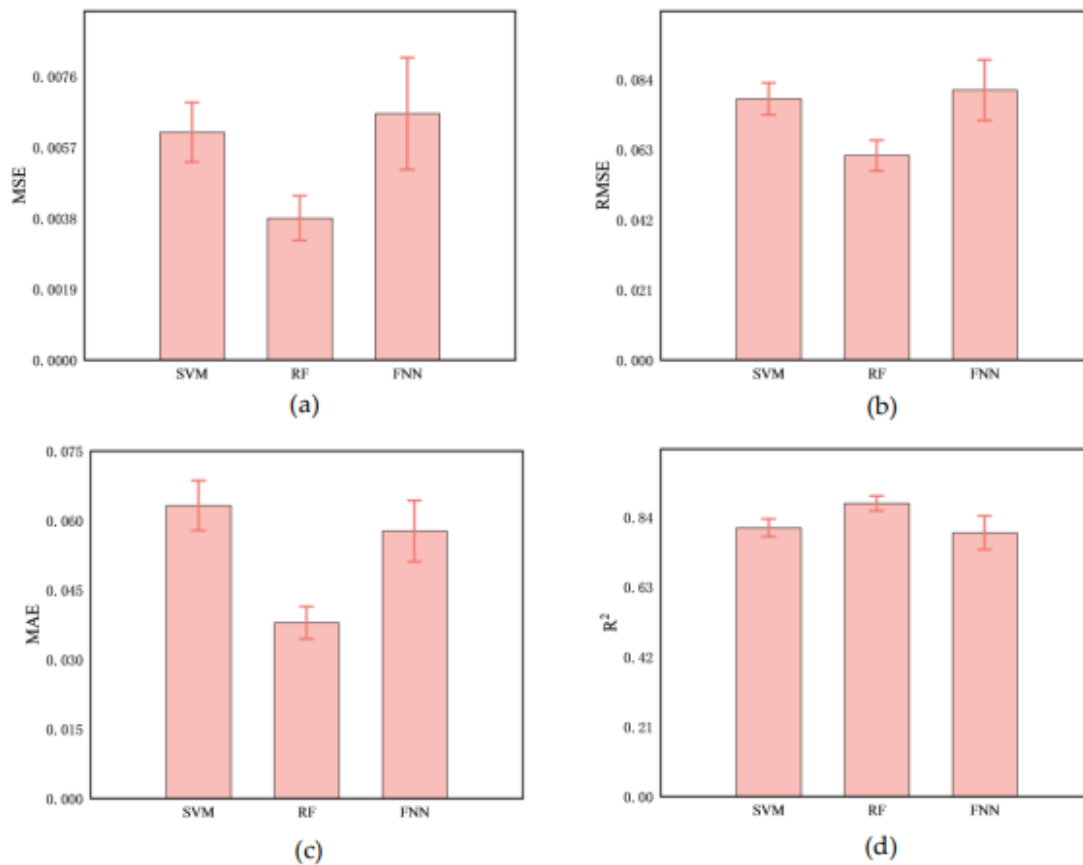


Figure 7. Comparison of predictive performance of three models for cerebral infarction volume ratio.

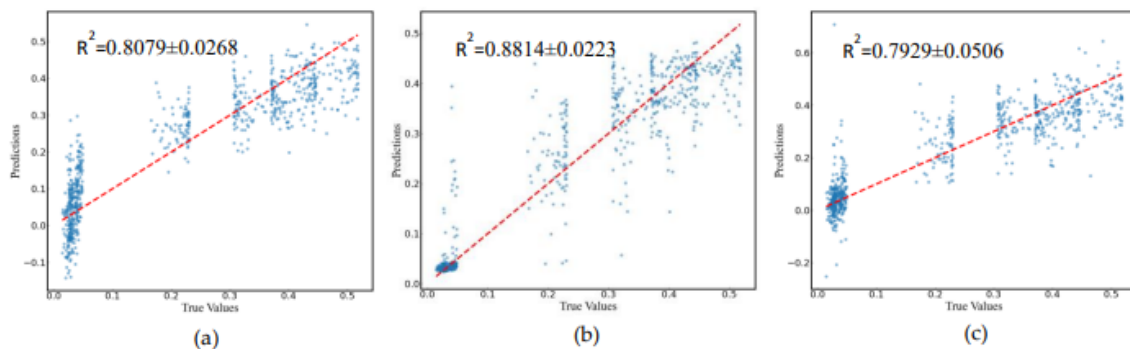


Figure 8. Prediction of cerebral infarction volume ratios using (a) SVM, (b) RF, and (c) FNN model.

4. Discussion

Cerebral edema is frequently associated with high rates of morbidity, mortality, and disability, making its severity a critical factor in patient prognosis. Especially for patients with stroke and traumatic brain injury, real-time continuous monitoring is essential. Ultrasound technology is particularly promising for bedside and wearable monitoring. Kreft et al. rapidly detected intracranial hypertension using ultrasonic time-harmonic elastography, at a shear wave speed (SWS) cutoff value of 1.67 m/s with specificity and sensitivity of 94% and 100% for the clinical ICP criteria of 25 cmH₂O [22]. Additionally, a conformal ultrasound patch has been applied for transcranial volumetric imaging and cerebral hemodynamic monitoring [23], underscoring the vital information in the early diagnosis and monitoring of central nervous system (CNS) diseases.

In this study, features of ultrasound echo signals with machine learning were combined to enable non-invasive monitoring and classification of cerebral edema. Sixteen features of ultrasonic echo signal related to the development of cerebral edema were extracted. It is worth noting that the wide distribution and presence of outliers in some features (see Figure 2) may be attributed to the rats' fixation on the plate during data acquisition, a necessary step to prevent mortality from multiple anesthesia sessions within a 24-hour period. However, the respiration and movement of rats may also lead to large feature variability and affect classification and prediction results.

The observed feature changes may correlate with alterations in the acoustic properties of brain tissue. Notably, the maximum value in the time domain showed a gradual decrease over time (see Figure 2a). In the early stage of cerebral edema, the influx of sodium ions, chloride ions, and water from the extracellular space into brain cells increases cell volume and tissue density, leading to higher acoustic impedance [4,6,24]. This increase enhances the reflection coefficient at the interface between edematous and normal brain tissue, resulting in stronger echoes. Pressure increases on an elastic medium are known to raise its density and ultrasound echo amplitude [25]. Interestingly, our study found a gradual decrease in the averaged maximum amplitude of echos from the cerebral edema within the first three hours, significantly different from the 0-hour mark ($p < 0.05$). This may be due to the aforementioned movement and respiration error. With the progress of cerebral ischemia increases, the blood-brain barrier becomes compromised, creating trans-endothelial permeability channels that allow water and certain plasma proteins to leak into the brain interstitium [4,6,24]. This leads to a decrease in brain cell volume (even cell rupture), brain tissue density, and acoustic impedance. Discrepancies in acoustic impedance are widely utilized in diagnosis [26–28]. High-frequency acoustic impedance imaging distinguishes between normal and cancerous breast cells with statistically different average impedance values (1.636 ± 0.010 MRayl vs. 1.612 ± 0.006 MRayl) [26]. Ito et al. also found significant acoustic impedance variations among different pathological liver conditions [27].

TTC staining at nine time points over 24 hours post-cerebral edema onset revealed no distinct white ischemic brain tissue in the first three hours. Not until the sixth hour did significant white cerebral ischemic tissue occur. In comparison, another group observed obvious white ischemic brain tissue two hours after modeling [29], a difference that may be due to the type of emboli or modeling techniques used. The cerebral infarction ratio at 24 hours after successful modeling is similar to ours (49.57% vs. 48.2%), indicating the a successfully established model.

Due to different clinical treatment strategies for cytotoxic and vasogenic brain edema, distinguishing between these types is crucial for diagnosis. While electrical resistivity of brain tissue has been utilized to differentiate edema types, the invasiveness of this technology may limit its wide application [29]. An algorithm for extracting amplitude features from electromagnetic induction has been proposed to classify acute and chronic phases of cerebral edema in rabbits, with a sensitivity of 85.0% and a specificity of 91.0% [30]. Machine learning models, including linear SVM, rough DT, and Naïve Bayes, have achieved 93% accuracy in distinguishing between cytotoxic and vasogenic brain edema in mice based on cerebral hemodynamic parameters [31]. In this study, the effectiveness of individual features was analyzed for classifying cerebral edema. It is found that not all features achieved high accuracy. For example, Kurtosis alone achieved the classification accuracy of only 61.5% in the RF model. However, the synergistic utilization of multiple features improved classification accuracy, with four traditional machine learning models (SVM, LR, DT, and RF) achieving over 95% accuracy, superior to all methods mentioned above.

In the MCAO model, the cerebral infarction volume ratio is often used to assess the severity of ischemic cerebral edema because of their positive correlation [32]. Brain water content measured using the dry-wet weight method can also demonstrate the severity of cerebral edema, but there was no significant differences between each time point [33,34]. Moreover, without precise control of time and temperature, substantial systematic errors may arise. Thus, the cerebral infarction volume ratio was utilized in this study to predict the severity of cerebral edema. The RF model showed good regression performance in predicting the cerebral infarction volume ratio, with an average MSE and

R^2 of 0.0038 and 0.8814, respectively. This method has great potential for non-invasive monitoring of cerebral edema in clinical settings, either bedside or wearable design, but requires further validation.

There are some limitations in our study. Firstly, the limited sample size may affect statistical analysis results. Secondly, the pathogenic causes and progression of cerebral edema models established using different methods may vary significantly. The performance of our non-invasive monitoring and prediction model will be evaluated using more cerebral edema models in the future. Thirdly, the rats were monitored within 24 hours after the onset of cerebral edema. Long-term monitoring (e.g., 48 and 72 hours) would be beneficial. Finally, more recent and advanced deep learning models, such as recurrent neural networks (RNN) and long short-term memory networks (LSTM) [35,36], will be explored to further improve accuracy.

5. Conclusions

This study introduces a novel, non-invasive ultrasound method for the monitoring of cerebral edema. Sixteen features extracted from the ultrasound echo signals are indicative of cerebral edema progression. The integration of these features with machine learning algorithm enabled the classification of different cerebral edema types and the prediction of edema severity. The experimental results are very promising. The RF model demonstrated high accuracy in classifying cerebral edema with ACC of 0.979 ± 0.019 and AUC of 0.996 ± 0.005 . Moreover, it also effectively predicts the infarction ratio with an R^2 value of 0.8814 ± 0.0223 . The findings of this research highlight the potential of ultrasound technology, in conjunction with machine learning, for assessing the severity and differentiating the types of cerebral edema. This approach offers a new, non-invasive diagnostic and real-time monitoring tool for brain trauma, which could significantly aid in clinical decision-making and patient management.

Supplementary Materials: The following supporting information can be downloaded at the website of this paper posted on Preprints.org. We provided all brain HE stained raw sections.

Author Contributions: Conceptualization and methodology, S.Y.; investigation, data curation, formal analysis, S.Y. and Y.Y.; writing—original draft preparation, S.Y.; writing—review and editing, Y.Z.; funding acquisition and supervision, Y.Z. Both authors have read and agreed to the published version of the manuscript.

Funding: This research was funded by Entrepreneurship and Innovation Support Program for Overseas Students in Chongqing(cx2021102), Chongqing Human Resources and Social Security Bureau.

Institutional Review Board Statement: The study was conducted in accordance with the Declaration of Helsinki, and approved by the Institutional Animal Care and Use Committee (IACUC) of Chongqing Medical University (approval number, IACUC-CQMU-2024-0698, 10 October 2024), and the experiment was monitored by the Animal Experiment Review Committee of Chongqing Medical University. Furthermore, all procedures complied with the National Institutes of Health guidelines for the care and use of laboratory animals.

Informed Consent Statement: Not applicable.

Data Availability Statement: The original contributions presented in this study are included in the article and supplementary Materials, further inquiries can be directed to the corresponding author.

Acknowledgments: We thank National Engineering Research Center of Ultrasonic Medicine Center for its strong support.

Conflicts of Interest: The authors declare no conflicts of interest.

References

1. Liotta, E.M. Management of cerebral edema, brain compression, and intracranial pressure. *CONTINUUM: Lifelong Learning in Neurology* 2021, 27, 1172-1200.
2. Stocchetti, N.; Maas, A.I. Traumatic intracranial hypertension. *New England Journal of Medicine* 2014, 370, 2121-2130.
3. Han, W.; Song, Y.; Rocha, M.; Shi, Y. Ischemic brain edema: Emerging cellular mechanisms and therapeutic approaches. *Neurobiol Dis* 2023, 178, 106029.
4. Stokum, J.A.; Gerzanich, V.; Simard, J.M. Molecular pathophysiology of cerebral edema. *Journal of Cerebral Blood Flow & Metabolism* 2016, 36, 513-538.
5. Sulhan, S.; Lyon, K.A.; Shapiro, L.A.; Huang, J.H. Neuroinflammation and blood-brain barrier disruption following traumatic brain injury: pathophysiology and potential therapeutic targets. *Journal of neuroscience research* 2020, 98, 19-28.
6. Jha, R.M.; Kochanek, P.M.; Simard, J.M. Pathophysiology and treatment of cerebral edema in traumatic brain injury. *Neuropharmacology* 2019, 145, 230-246.
7. Hawryluk, G.W.; Citerio, G.; Hutchinson, P.; Kolias, A.; Meyfroidt, G.; Robba, C.; Stocchetti, N.; Chesnut, R. Intracranial pressure: current perspectives on physiology and monitoring. *Intensive care medicine* 2022, 48, 1471-1481.
8. Carney, N.; Totten, A.M.; O'Reilly, C.; Ullman, J.S.; Hawryluk, G.W.; Bell, M.J.; Bratton, S.L.; Chesnut, R.; Harris, O.A.; Kissoon, N. Guidelines for the management of severe traumatic brain injury. *Neurosurgery* 2017, 80, 6-15.
9. Lietke, S.; Zausinger, S.; Patzig, M.; Holtmanspötter, M.; Kunz, M. CT-Based Classification of Acute Cerebral Edema: Association with Intracranial Pressure and Outcome. *Journal of Neuroimaging* 2020, 30, 640-647.
10. Dai, M.; Wang, L.; Xu, C.; Li, L.; Gao, G.; Dong, X. Real-time imaging of subarachnoid hemorrhage in piglets with electrical impedance tomography. *Physiological Measurement* 2010, 31, 1229.
11. Hackett, P.; Yarnell, P.; Weiland, D.; Reynard, K. Acute and evolving MRI of high-altitude cerebral edema: microbleeds, edema, and pathophysiology. *American Journal of Neuroradiology* 2019, 40, 464-469.
12. Thiagarajah, J.R.; Papadopoulos, M.C.; Verkman, A. Noninvasive early detection of brain edema in mice by near-infrared light scattering. *Journal of neuroscience research* 2005, 80, 293-299.
13. Zhao, S.-L.; Jin, G.; Bai, Z.-L.; Chen, J.-B.; Li, M.-W.; Li, G.; Zhuang, W.; Liu, Y.-N.; Qin, M.-X. Twenty-four-hour real-time continuous monitoring of acute focal cerebral ischemia in rabbits based on magnetic inductive phase shift. *BioMedical Engineering OnLine* 2020, 19, 1-15.
14. Robba, C.; Goffi, A.; Geeraerts, T.; Cardim, D.; Via, G.; Czosnyka, M.; Park, S.; Sarwal, A.; Padayachy, L.; Rasulo, F. Brain ultrasonography: methodology, basic and advanced principles and clinical applications. A narrative review. *Intensive care medicine* 2019, 45, 913-927.
15. Maurer, M.; Shambal, S.; Berg, D.; Woydt, M.; Hofmann, E.; Georgiadis, D.; Lindner, A.; Becker, G. Differentiation between intracerebral hemorrhage and ischemic stroke by transcranial color-coded duplex-sonography. *Stroke* 1998, 29, 2563-2567.
16. Motuel, J.; Biette, I.; Srairi, M.; Mrozek, S.; Kurrek, M.M.; Chaynes, P.; Cognard, C.; Fourcade, O.; Geeraerts, T. Assessment of brain midline shift using sonography in neurosurgical ICU patients. *Critical care* 2014, 18, 1-8.
17. Schmid-Elsaesser, R.; Zausinger, S.; Hungerhuber, E.; Baethmann, A.; Reulen, H.-J. A critical reevaluation of the intraluminal thread model of focal cerebral ischemia: evidence of inadvertent premature reperfusion and subarachnoid hemorrhage in rats by laser-Doppler flowmetry. *Stroke* 1998, 29, 2162-2170.
18. Koizumi, J. Experimental studies of ischemic brain edema. 1. A new experimental model of cerebral embolism in rats in which recirculation can be introduced in the ischemic area. *Jpn. J. Stroke*. 1986, 8, 1-8.
19. Longa, E.Z.; Weinstein, P.R.; Carlson, S.; Cummins, R. Reversible middle cerebral artery occlusion without craniectomy in rats. *stroke* 1989, 20, 84-91.
20. Swanson, R.A.; Morton, M.T.; Tsao-Wu, G.; Savalos, R.A.; Davidson, C.; Sharp, F.R. A semiautomated method for measuring brain infarct volume. *Journal of Cerebral Blood Flow & Metabolism* 1990, 10, 290-293.
21. Al Shalabi, L.; Shaaban, Z.; Kasasbeh, B. Data mining: A preprocessing engine. *Journal of Computer Science* 2006, 2, 735-739.
22. Kreft, B.; Tzschätzsch, H.; Shahryari, M.; Haffner, P.; Braun, J.; Sack, I.; Streitberger, K.-J. Noninvasive Detection of Intracranial Hypertension by Novel Ultrasound Time-Harmonic Elastography. *Investigative Radiology* 2022, 57, 77-84.
23. Zhou, S.; Gao, X.; Park, G.; Yang, X.; Qi, B.; Lin, M.; Huang, H.; Bian, Y.; Hu, H.; Chen, X. Transcranial volumetric imaging using a conformal ultrasound patch. *Nature* 2024, 629, 810-818.
24. Winkler, E.A.; Minter, D.; Yue, J.K.; Manley, G.T. Cerebral edema in traumatic brain injury: pathophysiology and prospective therapeutic targets. *Neurosurgery Clinics* 2016, 27, 473-488.

25. Zhu, L.; He, W.; Wu, J. Experimental Study of the Influence of Elastic Medium Deformation on Ultrasonic Propagation Characteristics. *Journal of Experimental Mechanics* 2014, 29, 26-32.
26. Fadhel, M.N.; Berndt, E.S.; Strohm, E.M.; Kolios, M.C. High-frequency acoustic impedance imaging of cancer cells. *Ultrasound in Medicine & Biology* 2015, 41, 2700-2713.
27. Ito, K.; Yoshida, K.; Maruyama, H.; Mamou, J.; Yamaguchi, T. Acoustic impedance analysis with high-frequency ultrasound for identification of fatty acid species in the liver. *Ultrasound in Medicine & Biology* 2017, 43, 700-711.
28. Meng, X.; Yi, Y.; Meng, Y.; Lv, G.; Jiang, X.; Wu, Y.; Yang, W.; Yao, Y.; Xu, H.; Bu, W. Self-enhanced acoustic impedance difference strategy for detecting the acidic tumor microenvironment. *ACS nano* 2022, 16, 4217-4227.
29. Song, J.; Chen, R.; Yang, L.; Zhang, G.; Li, W.; Zhao, Z.; Xu, C.; Dong, X.; Fu, F. Electrical impedance changes at different phases of cerebral edema in rats with ischemic brain injury. *BioMed Research International* 2018, 2018, 9765174.
30. Chen, J.; Li, G.; Liang, H.; Zhao, S.; Sun, J.; Qin, M. An amplitude-based characteristic parameter extraction algorithm for cerebral edema detection based on electromagnetic induction. *BioMedical Engineering OnLine* 2021, 20.
31. Zhang, Y.; Qi, X.; Li, W.; Wan, M.; Ning, X.; Hu, J. Research on the classification of early-stage brain edema by combining intrinsic optical signal imaging and laser speckle contrast imaging. *Journal of Biophotonics* 2024, 17, e202300394.
32. Kuts, R.; Frank, D.; Gruenbaum, B.F.; Grinshpun, J.; Melamed, I.; Knyazer, B.; Tarabrin, O.; Zvenigorodsky, V.; Shelef, I.; Zlotnik, A. A novel method for assessing cerebral edema, infarcted zone and blood-brain barrier breakdown in a single post-stroke rodent brain. *Frontiers in neuroscience* 2019, 13, 1105.
33. Shigeno, T.; Brock, M.; Shigeno, S.; Fritschka, E.; Cervós-Navarro, J. The determination of brain water content: microgravimetry versus drying-weighing method. *Journal of Neurosurgery* 1982, 57, 99-107.
34. Keep, R.F.; Hua, Y.; Xi, G. Brain water content: a misunderstood measurement? *Translational stroke research* 2012, 3, 263-265.
35. Chadha, G.S.; Panambilly, A.; Schwung, A.; Ding, S.X. Bidirectional deep recurrent neural networks for process fault classification. *ISA transactions* 2020, 106, 330-342.
36. Quddus, A.; Zandi, A.S.; Prest, L.; Comeau, F.J. Using long short term memory and convolutional neural networks for driver drowsiness detection. *Accident Analysis & Prevention* 2021, 156, 106107.

Disclaimer/Publisher's Note: The statements, opinions and data contained in all publications are solely those of the individual author(s) and contributor(s) and not of MDPI and/or the editor(s). MDPI and/or the editor(s) disclaim responsibility for any injury to people or property resulting from any ideas, methods, instructions or products referred to in the content.